Polymer Journal (2019) 51:693–707
https://doi.org/10.1038/s41428-019-0178-3

ORIGINAL ARTICLE

# Effect of silica nanoparticle size on the mechanical strength and wellbore plugging performance of SPAM/chromium (III) acetate nanocomposite gels

Zahra Azimi Dijvejin[1] · Ahmadreza Ghaffarkhah[2] · Saeid Sadeghnejad[1] · Mohsen Vafaie Sefti[1]

Received: 1 October 2018 / Revised: 3 January 2019 / Accepted: 26 January 2019 / Published online: 6 March 2019


## Abstract

Cross-linked polymer gels are a new type of temporary plugging agent and are mainly used to control the leakage of fluid during drilling, completion, and workover operations. Improving the mechanical strength and plugging performance of these materials enables them to resist tough wellbore conditions (e.g., high pressure and high temperature). In this study, various concentrations and size of silica nanoparticles are introduced into the sulfonated polyacrylamide (SPAM)/chromium (III) acetate system to produce a nanocomposite with enhanced mechanical properties. First, the rheological behavior of gelant and viscoelastic properties of synthesized nanocomposites are investigated. Then, the surface chemistry and morphology of the synthesized gels is evaluated by Fourier transform infrared (FTIR) spectroscopy and field emission scanning electron microscopy (FESEM), respectively. Finally, the maximum sealing differential pressure for gels for temporary plugging of a wellbore is measured by applying differential pressure across the nanocomposite gel in a designed set-up. The results showed that the precrosslinking reaction and the gelant viscosity are directly related to the size and concentration of the silica nanoparticles as well as the wellbore temperature. Moreover, it is demonstrated that nanocomposites containing 20–30 nm sized particles have a higher mechanical strength and plugging capability in comparison to composites containing silica particles with sizes of 7–10 and 60–70 nm.

## Introduction

Temporary plugging agents are mainly used to control the leakage of working fluids into formations during drilling, completion, and workover operations [1–6]. For example, during drilling operations, a portion or all of the drilling fluids may enter into high permeable zones when the pressure of the drilling mud is higher than the formation pressure. This results in the loss of several hundred barrels of expensive drilling fluids and a reduction in the productivity from underground formations [7, 8]. Temporary plugging agents can be used to isolate these high permeable subterranean zones from drilling fluids (Figs. 1a and c) [9, 10]. Temporary plugging agents can also be used to isolate the production sections of wells during maintenance or completion operations (Figs. 1b and d) [11–13]. In this case, equipment can be safely moved into and out of wells, and the high-pressure reservoir fluids can pose no threat to the safety of well personal and equipment [14, 15].

Temporary plugging agents should have a high and durable mechanical strength in the harsh conditions of oil and gas wells [16, 17]. In addition, these agents should not penetrate a long distance into production zones [8, 13, 18]. These materials can be classified into four groups: temporary plugging particles [7], degradable plugging agents [19], cement plugs [20], and cross-linked polymer gels [17].

Temporary plugging particles and degradable plugging agents consist of solid particles that are carried by drilling fluids into wells (Fig. 1a). The main difference between these two agents is that degradable plugging agents are made of natural materials, and as a result, they are environmentally friendly [21–23]. The main shortcoming for these two materials is that their performance mainly depends on their particle-size distribution [7, 24–27].

✉ Saeid Sadeghnejad
sadeghnejad@modares.ac.ir

[1] Department of Petroleum Engineering, Faculty of Chemical Engineering, Tarbiat Modares University, Tehran 14115-111, Iran

[2] Research Institute of Petroleum Industry (RIPI), West Blvd., Near Azadi Sports Complex, Tehran 14857-33111, Iran

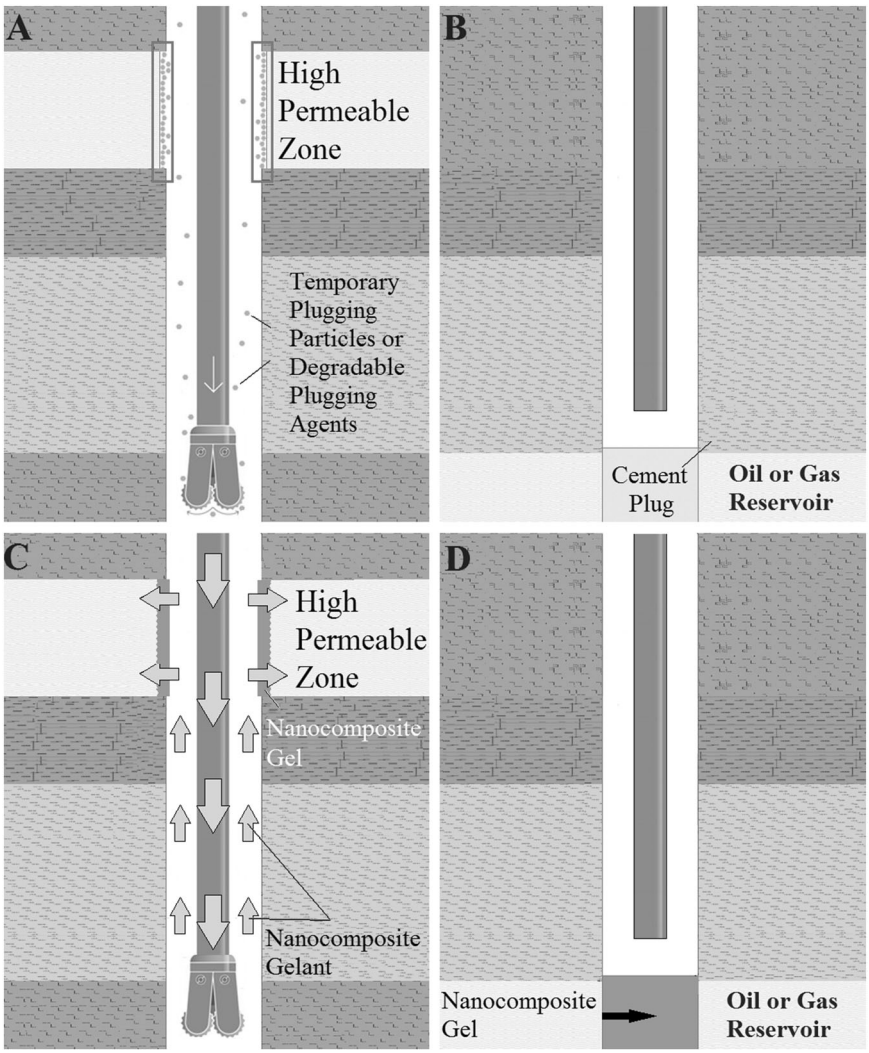


**Fig. 1** Schematic for the control of the leakage of workover fluids into formations using temporary plugging agents. (**a**) Using temporary plugging particles or degradable plugging agents to isolate high permeable zones, (**b**) using a cement plug to isolate the production section of wells, (**c**) using a nanocomposite gel to isolate high permeable zones, and (**d**) using a nanocomposite gel to isolate the production section of wells

However, the available models that are routinely used to calculate suitable particle sizes mainly depend on the pore-throat diameter without considering other important parameters such as complex pore-throat structure of the formation [28–32].

Cement plugs are usually used for temporary close-in operations in perforated parts of wells [13, 33]. When the cement slurry reaches its target location, it isolates the production zone (Fig. 1b) [34, 35]. Despite wide application in the petroleum industry, some problems remain with cement hardening [36]. Furthermore, in many cases, cement can mix with drilling fluids and lose its mechanical strength [37, 38]. Moreover, cement might also react with chemicals that are available in underground formations, such as $CO_2$, and lose its mechanical strength [39–41].

Nanocomposite gels can be used as a new way to isolate high permeable zones during drilling (Fig. 1c) or block the production sections of drilling wells (Fig. 1d). Due to the aforementioned shortcomings of routine plugging agents, developing high-performance cross-linked gels is highly desirable. For isolating a target zone, a nanocomposite gelant is injected into wells. When it reaches its target location, it cures the well under high-pressure and high-temperature conditions and eventually blocks the high permeable zones or production section of the well [1, 4, 6, 13].

The main components of cross-linked gels are a polymer and water soluble cross-linker [42–44]. When cross-linkers are connected to polymer chains, a three-dimensional gel network or cross-linked gel is formed [20, 45, 46]. Many researchers have studied the plugging performance of cross-linked gels [47–52]. Jia and Chen proposed a $Cr^{+3}$/salt-tolerant polymer gel to reduce fluid loss in porous formations [53]. Zhao et al. discussed a temporary plugging agent based on a polymer gel to isolate highly permeable zones in acidizing processes [1]. Imran et al. introduced a novel polymer gel that has potential to plug porous formations. Good injectivity, high plugging ability, and low formation damage were found to be the most important characteristics of this gel [54]. In another study by Hajipour et al., a new cross-linked gel system was synthesized based on a

polyacrylamide sulfonated copolymer and chromium (III) acetate. Based on a series of experiments, it was concluded that the abovementioned synthesized cross-linked gel could be used for close-in well operations [13].

Cross-linked gels and their plugging performance mainly depend on the type of polymers and cross linkers used and the interaction between different components of cross-linked gels. However, most conventional cross-linked gels are weak and have a low mechanical performance [55, 56]. Many methods such as using two independent cross-linkers [57], adding nanoparticles to a polymer/cross linker system [56], and utilizing a topologically interlocked none-covalent cross linker [58] have been used to improve the mechanical properties of cross-linked gels. Among them, nanocomposite gels that utilize inorganic nanoparticles to form cross-linking junks in gels have received much attention [56]. Such nanocomposite gels consist of an organic polymer and an inorganic nanoparticle and were first introduced by Haraguchi and Takehisa in 2002 [59]. Consequently, many studies have used different nanoparticles such as nanocellulose, clay, silica, and magnesium silicate as an inorganic component in polymer/cross-linker systems to improve their performance [60–65]. For example, Wu et al. synthesized a polyacrylamide /silica nanocomposite via an in situ free-radical polymerization method. Their results showed that the compression strength and elastic modulus of the synthesized gels are significantly improved by adding nanosilica particles [66]. Zhao et al. showed that use of cellulose nanocrystals could effectively improve the mechanical properties of a poly(2-hydroxyethylmethacylate) (PHEMA) gel [67]. Dijvejin et al. showed that the introduction of magnesium silicate nanocrystals into the HPAM/chromium (III) acetate system produced a nanocomposite gel with enhanced mechanical properties [56].

In this study, twelve different SPAM/chromium (III) acetate nanocomposite gels are synthesized based on various concentrations and sizes of silica nanoparticles. First, the rheological behavior of the gelant solution composed of silica nanoparticles with varying size and concentration is investigated at different temperatures. Subsequently, the viscose and elastic moduli of the synthesized nanocomposites are evaluated to determine the effect of the nanoparticle size and concentration on the gel mechanical properties. The surface chemistry and morphology of the synthesized gels are evaluated by using FTIR spectroscopy and the FESEM method, respectively. Finally, the differential compressive loading of the gels is investigated under a wellbore condition by designing a novel set-up. This approach enables us to measure the maximum differential pressure that can be tolerated by different nanocomposite gels before gel failure.

## Experimental section

### Materials

SPAM with an average molecular weight of 8 million Dalton and sulfonation degree of 25% from the SNF company (France), under the trade name of AN125, was used to make the nanocomposite gel system. The structure of this polymer is shown in Fig. 2. The sulfonic acid ($-SO_3^-$), amide ($-CONH_2$), and carboxylate ($-COO^-$) groups are the cross-linkable chemical groups for these polymers [68–70]. As a cross-linker, chromium (III) acetate (Sigma Aldrich, USA), in the form of dark green powder, was implemented during gel preparation. The nanoparticle used in this study is SiO2 nanopowder (US Research Nanomaterials, Inc, USA) with three different diameter ranges of 7–10, 20–30 and 60–70 nm. To consider the impact of salinity on the gel properties, the formation water from one Iranian reservoir (i.e., Sarvak) was synthetically made in this study. All salts were purchased from Sigma Co. The brine analysis for Sarvak formation is shown in Table 1.

### Synthesis of nanocomposite hydrogels

In this study, 12 nanocomposite gels (Table 2) with different sized SiO2 nanopowder were synthesized according to the following steps. First, nanosilica powder was gently added to deionized water under continuous stirring. The solution was sonicated via an ultrasonic bath for 15 min.

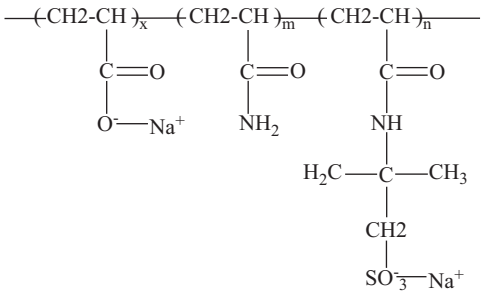


**Fig. 2** The chemical structure of SPAM

**Table 1** The water composition of Sarvak formation brine

| Component | Value (mg/L) | Component | value (mg/L) |
|---|---|---|---|
| $Na^+$ | 66,621 | $Sr^{2+}$ | 1,390 |
| $K^+$ | 2579 | $HCO_3^-$ | 632 |
| $Ca^{2+}$ | 2875 | $Cl^-$ | 131,165 |
| $Mg^{2+}$ | 5500 | $SO_4^{2-}$ | 62 |
| $Ba^{2+}$ | 1402 | $NO_3^-$ | 352 |
| Total dissolved solid (TDS) | 224,386 | | |

**Table 2** Chemical composition of the synthesized nanocomposite gels

| Gel sample code | Nanosilica concentration (Wt. %) | Diameter of nanosilica particles (nm) |
|---|---|---|
| Gel 1 | 0.25 | 7–10 |
| Gel 2 | 0.50 | 7–10 |
| Gel 3 | 0.75 | 7–10 |
| Gel 4 | 1.00 | 7–10 |
| Gel 5 | 0.25 | 20–30 |
| Gel 6 | 0.50 | 20–30 |
| Gel 7 | 0.75 | 20–30 |
| Gel 8 | 1.00 | 20–30 |
| Gel 9 | 0.25 | 60–70 |
| Gel 10 | 0.50 | 60–70 |
| Gel 11 | 0.75 | 60–70 |
| Gel 12 | 1.00 | 60–70 |

Then, the silica suspension was stirred for 30 min to achieve a homogeneous dispersion. Next, SPAM powder (2.6 wt%) was slowly added to the suspension with continuous stirring for 4 h to obtain a homogeneous solution. Chromium (III) acetate (0.26 wt%) was also mixed with the polymer suspension at room temperature using a magnetic stirrer for 15 min. Finally, the nanocomposite gels were prepared by keeping the gelant solution in an oven at 90 °C for 9 h.

## Bottle tests

The bottle tests, as a semiquantitative experimental approach, were used to investigate the gelation rate and gel strength of the synthesized polymer gels (Table 2). To evaluate the optimum concentration of the polymer and cross-linker, several polymer gels (without any nanoparticles) were synthesized with different polymer concentrations (i.e., 15000, 20000, 26000, and 32000) and various cross-linker/polymer ratios (1/20, 1/10, and 1/5) at 90 °C and a pH of 8.5. The prepared samples were then placed into an oven at 90 °C for 300 h. Eventually, the hydrogel strength was recorded based on alphabetic codes (A, B, C, D, and E: Fluid hydrogel; F, G, and H: Nonfluid hydrogel; I and G: Gel) [13, 53, 71].

## FESEM measurements

An FESEM Hitachi S-4800 (Japan) was used to investigate the morphology of various synthesized samples. The FESEM tests were carried out on dried and ground samples. In this study, a high vacuum oven at 90 °C was used to dry all nanocomposite samples. Furthermore, great visual depth with three-dimensional appearance for all the samples was obtained when the dried samples were coated by a conductive coating material (i.e., gold).

## FTIR measurements

FTIR spectroscopy was used to characterize the chemical bonds of the synthesized nanocomposites. The absorption spectra for the dried and ground nanocomposite samples were obtained using a VERTEX 70 Spectrometer (Bruker, Germany) in transmission mode.

## Rheology of the gelant

In this study, the rheology of the gelants (i.e., nanocomposite system before gelation) was measured using a QC lab (RheolabQC, Anton Paar, Germany). The gelant viscosity for all the nanocomposite gels was measured at a constant shear rate of 10 1/s.

## Viscoelasticity measurements for the nanocomposite gels

The viscoelastic properties of the synthesized nanocomposite gels, including the elastic modulus (G′) and viscous modulus (G″), were measured by using a MCR300 Rheometer (Anton-Paar GmbH, Germany). To carry out the rheological tests, the synthesized polymeric gel samples were prepared and aged for 90 h at 90 °C, and then, the rheological measurements were conducted by oscillatory measurements [56, 72, 73].

## Performance evaluation for wellbore plugging using nanocomposite gels

In this study, an experimental setup was designed to determine the maximum differential compressive pressure (DCP) that the synthesized nanocomposite gels can tolerate before failing. The schematic for this experimental setup is shown in Fig. 3. The main parts of the setup are a holder cylinder with varying diameters of 6.35, 12.7, 25.4, and 50.8 mm and a fixed length of 304.8 mm, a thermal jacket for fixing the cylinder temperature, an injection pump (Petro-Azma Co., Iran), and a transfer vessel. The injection pump was able to inject at a constant flow rate (in the range of 0.01 and 32 cc/min) or pressure (up to 100 bar).

To perform experiments, a 1-inch sand bed was embedded at the bottom of the holding cylinder (at flow upstream) to ensure a uniform distribution for the nanocomposite gels. After that, the nanocomposite gelant was placed above this sand bed. The temperature of the thermal jacket was then set at 90 °C. After spending sufficient time, the nanocomposite gel was formed. Subsequently, the remaining portion of the cylinder was filled with diesel fuel, which can simulate the operational condition of the gel as a plugging agent under wellbore conditions (i.e., on one side,

it is in contact with a reservoir fluid, and on the other side, it is in touch with a workover fluid).

To determine the maximum DCP before nanocomposite failure, the formation water was injected from the bottom of the cylinder at a constant rate of 10 cc/min. Since the middle section of the cylinder is blocked by the gel column, the upstream pressure could be gradually increased up to a pressure at which the gel integrity breaks and cannot tolerate the DCP across it. Finally, the maximum upstream pressure (i.e., equal to DCP) is recorded just when the diesel fuel is seen downstream of the cylinder.

## Results and discussion

### Selecting the optimum polymer and cross-linker concentrations

To find the optimum concentration for the polymer and cross-linker, several gel polymers were investigated by using the bottle test method. The outcomes for these tests are shown in Table 3. The results indicated that by increasing the polymer concentration, the strength of the polymer gels improves (by changing the concentration of polymer from 1500 to 26,000 ppm, the final gel code changed from G to I). However, when the polymer concentration exceeded 26,000 ppm, the gelation process occurred very fast (less than 0.5 h). Immediate gelation reduces the plugging performance of the polymer gel system and creates lots for gelant pumping [53, 54]. Therefore, the optimum concentration for the polymer was selected to be 26,000 ppm.

The results also indicate that by increasing the cross-linker/polymer ratio, the gel strength increases because by increasing the cross-linker/polymer ratio, the number of cross-linking bonds increases, which in turn results in an improvement in the polymer gel strength [56, 74, 75]. However, when the cross-linker/polymer ratio reached 1/5, gel syneresis occurred, and water was removed from the gel network. Eventually, optimum values for the polymer concentration and cross-linker/polymer ratio were selected

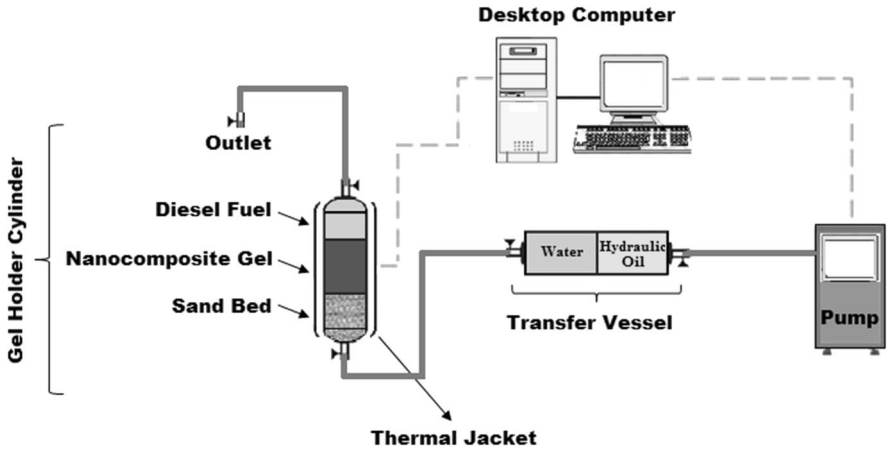


**Fig. 3** Schematic of the gel differential compressive pressure setup

**Table 3** The results obtained from bottle tests for various polymer gels

| SPAM concentration (ppm) | Cross-linker /polymer weight concentration ratio | Gel strength code after different aging times (hours) | | | | | | | | |
|---|---|---|---|---|---|---|---|---|---|---|
| | | 0.5 | 1 | 3 | 9 | 12 | 24 | 90 | 150 | 300 |
| **15,000** | 1/20 | A | A | A | B | C | E | F | F | G |
| | 1/10 | A | A | B | C | C | F | F | F | G |
| | 1/5 | A | A | C | C | C | F | F | G | G |
| **20,000** | 1/20 | A | B | B | C | E | F | G | G | H |
| | 1/10 | A | B | C | C | F | F | G | G | H |
| | 1/5 | A | B | C | F | F | G | G | H | H |
| **26,000** | 1/20 | A | B | C | E | F | G | G | I | I |
| | 1/10 | A | C | C | F | G | I | I | I | I |
| | 1/5 | C | C | F | F | F | G | G | I | I |
| **32,000** | 1/20 | C | F | G | G | I | I | I | I | I |
| | 1/10 | C | F | G | I | I | I | I | I | S |
| | 1/5 | C | G | G | I | I | I | I | I | S |

to be 26,000 ppm and 1/10, respectively, and used for the synthesis of various nanocomposites in the following analyses.

## Rheological behavior of the gelant

The viscosities of the gelant-solutions with different nanoparticle sizes and concentrations at 90 °C and a shear rate of 10 1/s were measured, as shown in Fig. 4. The sudden rise in the gelant viscosity at preliminary times (shown by the blue rectangle in Fig. 4) shows the formation of a precrosslinking in the gel and the start of the gelation process. As can be seen from Fig. 4 for all nanoparticle sizes, the maximum viscosity of the gelant-solutions (at later times) is increased by increasing the nanoparticle concentration. Moreover, gels with higher nanoparticle concentrations show a delayed precrosslinking reaction (blue rectangle in Fig. 4). This finding is mainly because silica particles react with the chrome ions of the chromium (III) acetate. This reaction reduces the reaction rate between the polymer and cross-linker, which in turn results in a slower gelation process [76]. It is also observed from Figs. 4a to c that the viscosity of the gelant-solution at late-time increases by reducing the nanoparticle size. Furthermore, under this condition, the precrosslinking reaction is postponed to later times. It should be noted that when the nanoparticle size is reduced, the reaction between chrome ions and silica particles increases. This results in a slower reaction among polymer chains and the cross-linker.

Figure 5 depicts the gelant-viscosity of different nanoparticle sizes at various temperatures and constant shear rate of 10 1/s. As seen, the gelation process is retarded for a reduced temperature. As a result, at low temperatures (e.g., surface temperature) the viscosity of the gelant is low, while at higher temperature (e.g., 90 °C), the gelation process speeds up. Thus, in an operation at wellsides, gelants can be easily pumped into the wellbore. While the gelants proceed into deeper depths, the wellbore temperature increases; therefore, the gelation process speeds up, and the gelant is turned to a solid gel, which prevents filtration of the gelants into the formation and damage to the production zones.

## Rheological behavior of the nanocomposite gel

The strength and adhesion of the nanocomposite gels were evaluated by measuring the elastic modulus (G′) and the viscous modulus (G″). By increasing the viscoelastic moduli, the ability of a gel to resist deformation and compression increases. Fig. 6 shows that the elastic and viscous moduli for the synthesized gels are sensitive to the size and concentration of silica nanoparticles. The results demonstrated that for increasing nanoparticle concentration, both G′ and G″ significantly increases. This rise in the viscoelastic modulus of the gels demonstrates a strong interaction between the gel network and silica nanoparticles. It is worth mentioning that the nanosilica increases the viscous resistance between shearing layers, which results in decreasing fluidity for free water trapped in the gel network. Therefore, the mechanical strength of the nanocomposite gels is improved by increasing the nanoparticle content.

The viscoelastic modulus for the gels containing nanoparticles with sizes of 20–30 nm (Fig. 6b) was much higher than that for the composites with nanosilica particle sizes of 7–10 nm (Fig. 6a) and 60–70 nm (Fig. 6c). By decreasing the nanoparticle size, the interaction between the polymer segments and nanoparticle surface increases, which forces the polymer chains to wrap tightly to the silica nanoparticles, resulting in the formation of stronger gel networks [77–79]. This result is why the nanocomposites containing particles with sizes of 20–30 nm have much higher values for G' and G" compared to gels with 60–70 nm particles. However, when the size of the nanoparticle decreases further (e.g., 7–10 nm), the aggregation/agglomeration level in the nanocomposites increases [80, 81].

## FTIR analysis

In this section, the surface chemistry for the gel numbers 4, 8, and 12 (refer to Table 2) was investigated by FTIR measurements within the mid infrared region (i.e., 400–4000 $cm^{-1}$). In Fig. 7(a), the broad peak at 3700–3000 $cm^{-1}$ is assigned to the stretching vibrations of the O–H and N–H groups. Other peaks at 2942, 1700, 1666, and 1410 $cm^{-1}$ are attributed to stretching vibrations of C–H, C=O (carboxylic acid), C=O (amid), and the C–N bands of HPAM [82, 83]. The peaks at 1200 and 1038 $cm^{-1}$ (i.e., assigned to O=S=O group) and the peak at 628 $cm^{-1}$ (i.e., assigned to S–O group) are due to the sulfonation of the HPAM (SPAM). Moreover, the peaks at 466, 808, and 1106 $cm^{-1}$ are attributed to the stretching and bending vibrations of the Si–O–Si and Si–O groups that represent the availability of the silica nanoparticles in the samples [84, 85]. The peak centered near 3440 $cm^{-1}$ is attributed to the OOH vibration that does not participate in hydrogen bonding (i.e., free OOH stretching vibration), and the other peak approximately 3200 $cm^{-1}$ is assigned to hydrogen-bonded OOH groups [86–89].

FTIR spectroscopy can also be a useful analytical method for examining intermolecular hydrogen bonding [90]. To quantify the hydrogen bonding formed, the absorbance values were calculated using equation 1 [90–93],

$$Abs = 2 - Log(T\%) \quad (1)$$

where Abs is the absorbance and T is the percent transmittance. Then, the ratio of the absorbance of the

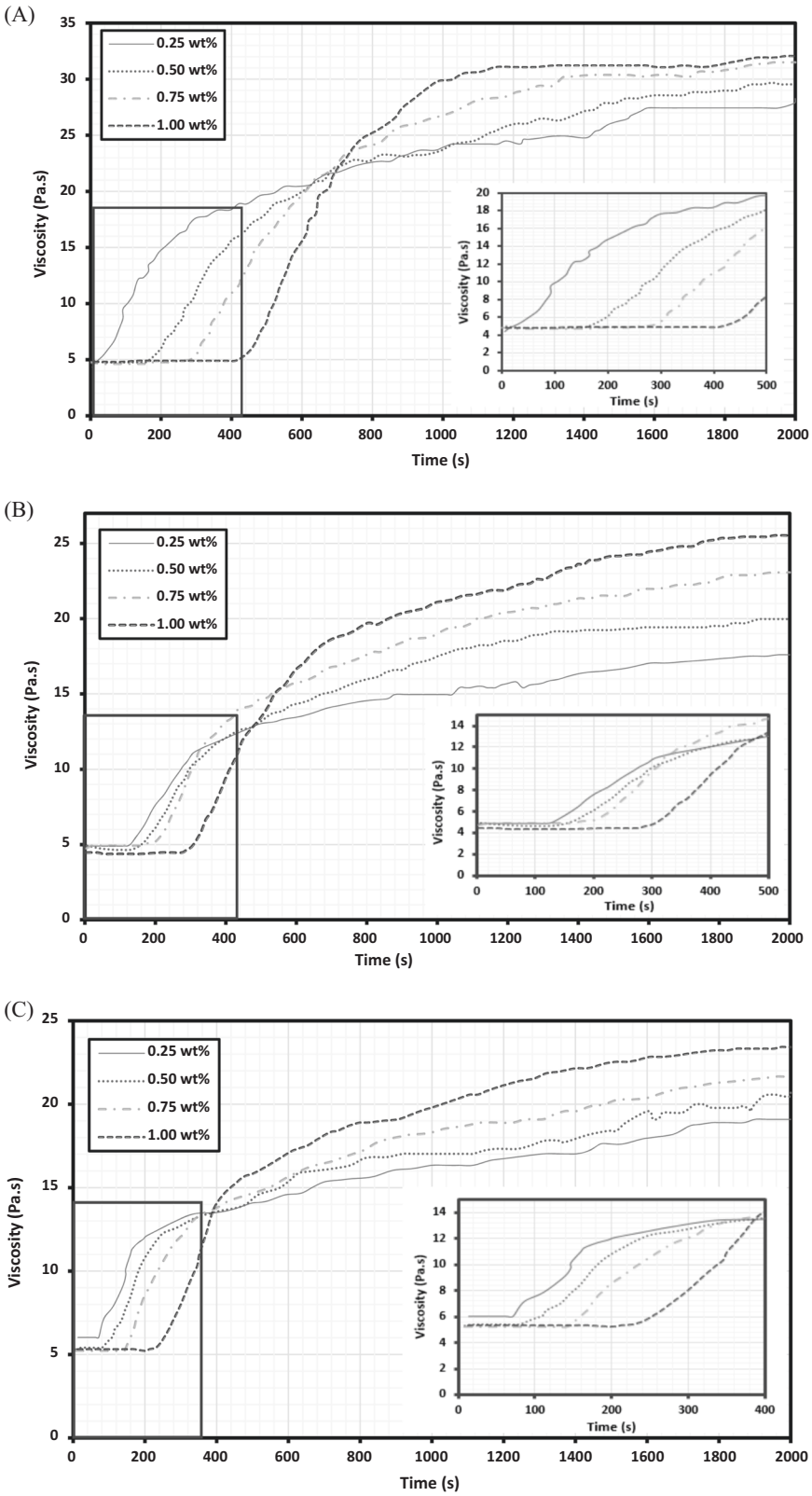


**Fig. 4** The gelant-solution viscosity for (**a**) 7–10 nm, (**b**) 20–30 nm, and (**c**) 60–70 nm nanoparticles concentrations at 90 °C and a shear rate of 10 1/s

nanocomposites at 3200 and 3440 $cm^{-1}$ (i.e., assigned to H-bonded OOH vibrations and free OOH vibrations, respectively) was utilized to calculate the relative absorbance ($Abs_{rel}$) using equation 2 [90–93],

$$Abs_{rel} = Abs_{3200}/Abs_{3440} \quad (2)$$

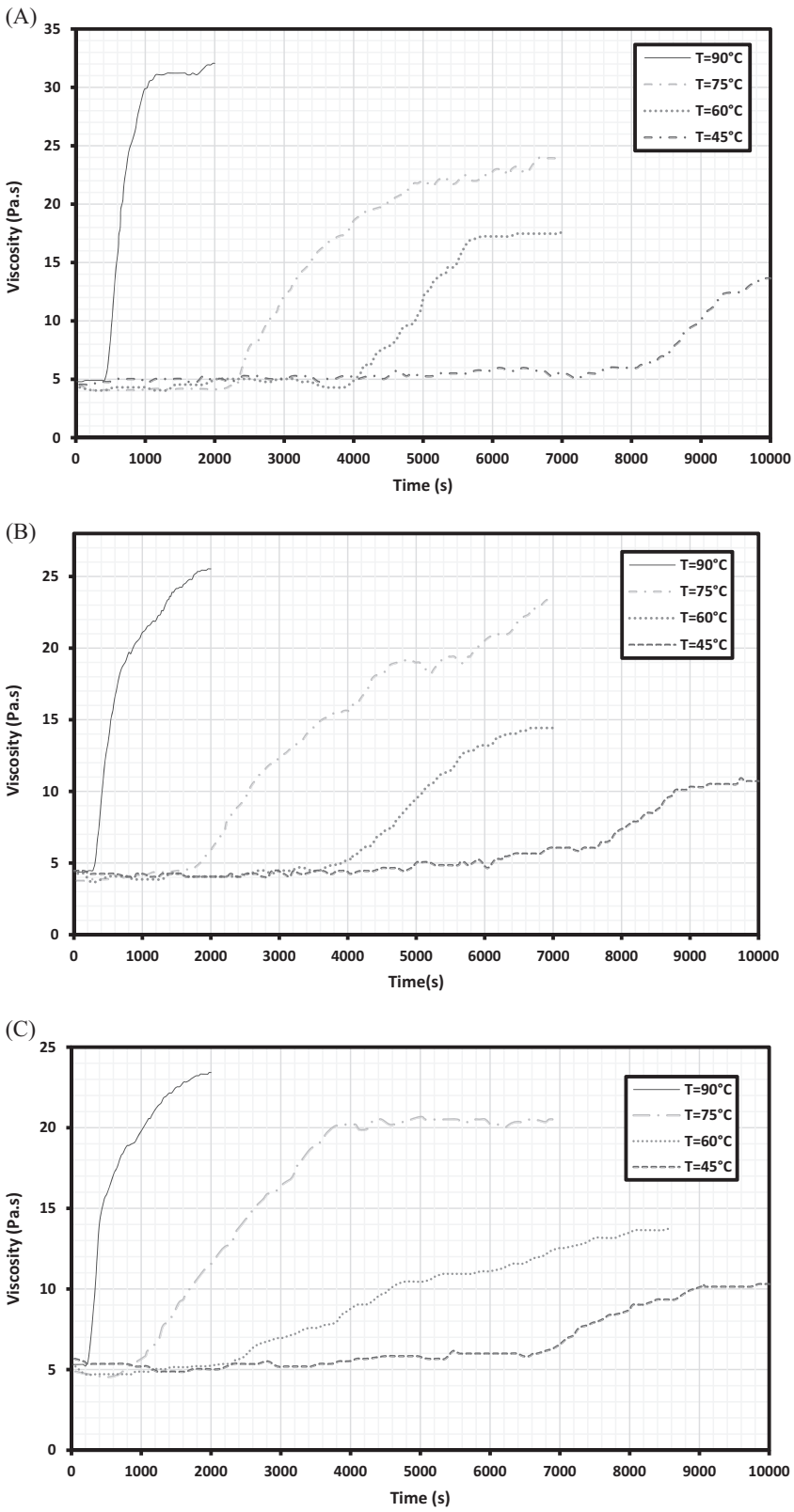


**Fig. 5** The gelant-viscosity for (**a**) 7–10 nm, (**b**) 20–30 nm, and (**c**) 60–70 nm nanoparticles at various temperatures (45, 60, 75, and 90 °C) and a constant shear rate of 10 1/s

Here, $Abs_{rel}$ is the relative absorbance. $Abs_{3200}$ and $Abs_{3440}$ are the absorbance of the bond around the wavenumber of 3200 and 3440 $cm^{-1}$, respectively. Fig. 7(b) compares the relative absorbance of all three nanocomposites. The greater value of the relative absorbance for the nanocomposite with particle size of 20–30 nm could be related to the larger

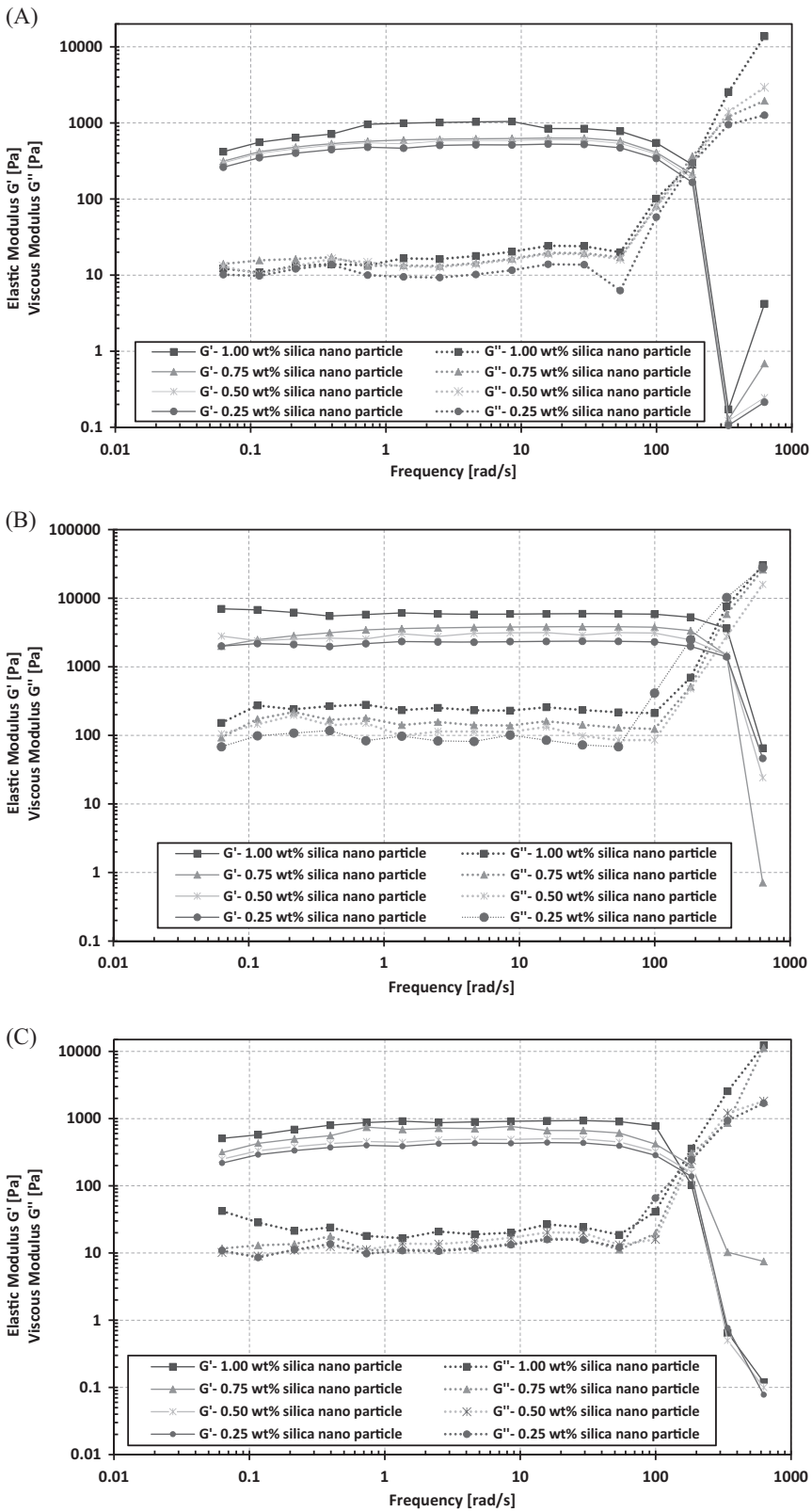


**Fig. 6** The elastic and viscous moduli of synthesized gels containing (**a**) 7–10 nm (**b**) 20–30 nm, and (**c**) 60–70 nm nanoparticles

number of H-bonded OOH groups available in this nanocomposite. In addition, the FTIR spectrum for the nanocomposites in the range of 4000–3000 $cm^{-1}$ in the absorbance scale is shown in Fig. 7 (c). It can be seen that maximum peak for the H-bonded OOH group is shifted from 3238 $cm^{-1}$ (for 60–70 nm) to 3204 $cm^{-1}$

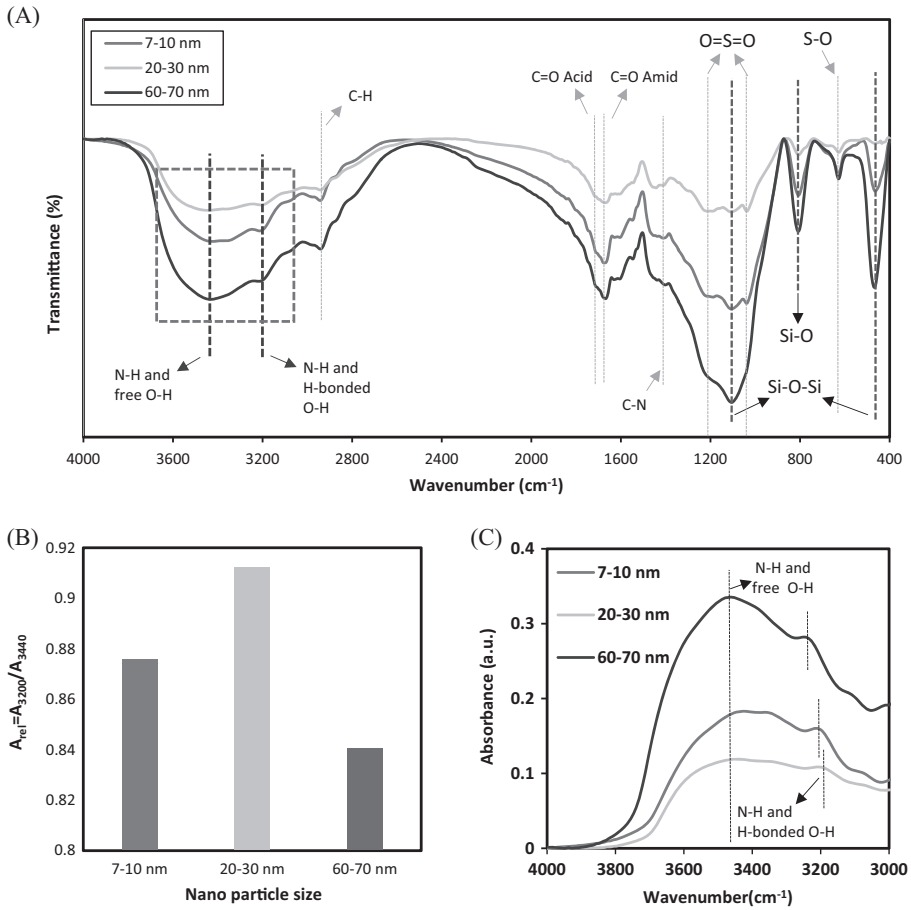


**Fig. 7** **a** The FTIR spectra for three different nanocomposites with different sizes of silica nanoparticles (gels numbered 4, 8 and 12 from Table 2). The peaks for the base polymer (SPAM) and nanoparticles are shown with blue dotted lines and black dash-dotted lines, respectively. The red dashed lines show free O–H and H-bonded O–H peaks. **b** Effect of nanoparticle size on the relative absorbance, $Abs_{rel}$, of the nanocomposite FTIR spectra, **c** Scale-expanded FTIR spectra based on absorbance vs. wavenumber showing the band shift due to hydrogen bonding

(for 7–10 nm) and finally to 3188 $cm^{-1}$ (for 20–30 nm). This band shift to lower frequency is another indication of enhanced hydrogen bonding in the nanocomposite with particle size of 20–30 nm [89, 91]. These results are in confirmation with the viscoelastic behavior observed for the nanocomposites in the previous section, wherein the nanocomposite with nanoparticle size of 20–30 nm showed a higher viscoelastic modulus in comparison to the other samples.

## FESEM analysis

FESEM provides high-resolution surface imaging got the nanomaterials. Here, this method was used to compare the morphology of the base hydrogel without nanoparticles with nanocomposite gels that contained 1 wt% of silica nanoparticles of varying size. The FESEM images for gels numbered 4, 8 and 12 (refer to Table 2) and the base hydrogel gel without nanoparticles are shown in Fig. 8. As seen in this figure, the surface of the base hydrogel without nanoparticles (Fig. 8a) is rather smooth and homogenous. However, the nanocomposites containing 1 wt% of nano-silica of different sizes (Figs. 8b to 8d) show a rough surface. This result is mainly because the interaction between polymer segments and nanoparticles forces the polymer chains to wrap around the silica nanoparticles [64, 94, 95].

## Plugging performance evaluation for the nanocomposite gel

The effect of gel column length and diameter on the maximum DCP for gel number 8 (containing 1 wt% of 20–30 nm silica nanoparticles) is shown in Fig. 9. As seen from the data, by increasing the length and diameter of the gel column, the maximum DCP for the sample increases. This result is mainly because by increasing the gel column length and diameter, the entire weight of the gel system and the contact area between the gel and the body of the cylinder increases, which increases the adhesive force of the gel into the cylinder body, resulting in higher resistance of the gel system against pressure.

To investigate the effect of nanoparticle size on the maximum DCP of the synthesized nanocomposites, the ability of gel number 4, 8, and 12 to resist differential pressure was evaluated by the designed setup. Fig. 10 depicts the maximum DCP before the failure of gel numbered 4, 8 and 12 for different gel column diameters. The nanocomposite containing 20–30 nm particles has a higher

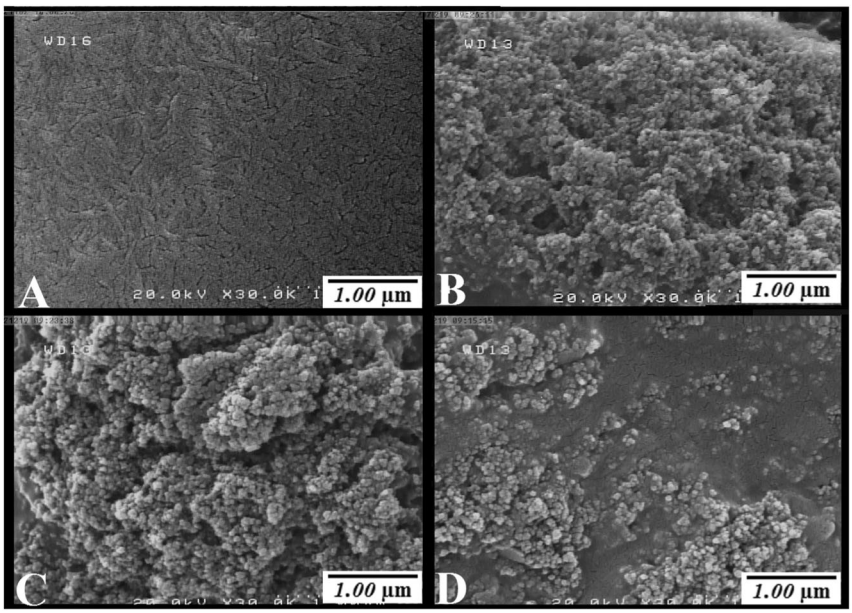


**Fig. 8** FESEM images of (**a**) the base hydrogel without nanoparticles and nanocomposite gels numbered (**b**) 4, (**c**) 8, and (**d**) 12 from Table 2

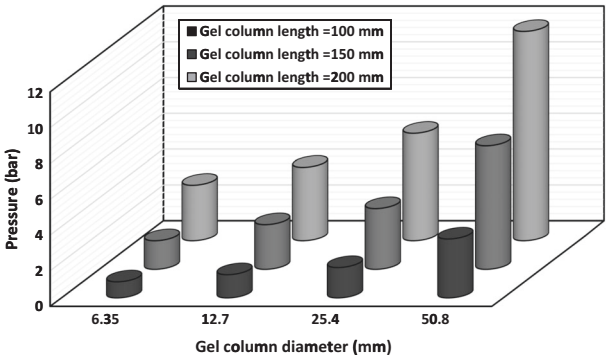


**Fig. 9** The effect of gel column length and diameter on the maximum DCP of gel number 8

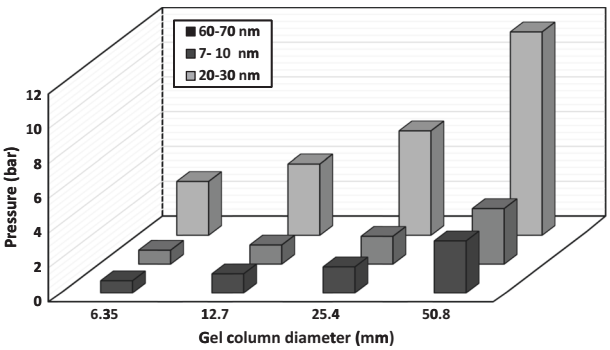


**Fig. 10** The maximum tolerable pressure of gels numbered 4, 8 and 12 for different gel column diameters. The gel length was kept fixed (200 mm) in all tests

DCP in comparison to the other gels, which is mainly because this gel has higher mechanical strength compared to the composites with particle sizes of 7–10 and 60–70 nm.

Figure 11 A shows the pressure-time behavior of the aforementioned gels during water injection. The nanocomposites containing 7–10 and 60–70 nm silica nanoparticles not only have a lower DCP but also break faster under lower pressure values. Fig. 11b shows the primary portion (next to the sand bed) of gel numbered 4, 8 and 12 after gel failure at maximum DCP. It should be noted that the gel column length for these samples was fixed at 200 mm and their diameter was 25.4 mm. Although the maximum DCP for gel number 4 and 12 was less than that for gel number 8, the amount of damage for gel number 8 was far less than that for the other composites when they reached their maximum DCP. This result again demonstrates that the nanocomposite containing 20–30 nm silica nanoparticles has better mechanical properties than the nanocomposites composed of 7–10 and 60–70 nm particles.

After finishing the DCP tests, we extracted the gel columns from the steel cylinder. Fig. 12 shows the gel form and shapes after finishing the DCP tests for gels numbered 4, 8, and 12 with nanoparticle sizes of 7–10, 20–30 and 60–70 nm, respectively. When gel number 4 and 12 reached their maximum DCP, a hole was created inside their gel column, and in addition, their gel columns were disconnected from the steel cylinder (i.e., representative of a wellbore casing). Furthermore, the gel column in these two cases was divided into several smaller pieces (Figs. 12a, c). This result shows that during gel failing at higher pressures, on top of gel breaking into smaller pieces, the cohesiveness of the gel to the wellbore casing breaks as well (i.e., the gel is detached from the wellbore). This is important as disconnection of the gel during workover operations means that the gel cannot not temporary plug the wellbore. However, for gel number 8, after reaching its maximum DCP, the injected fluid only breaks through a small hole in the body of the gel column, and the gel column is not detached

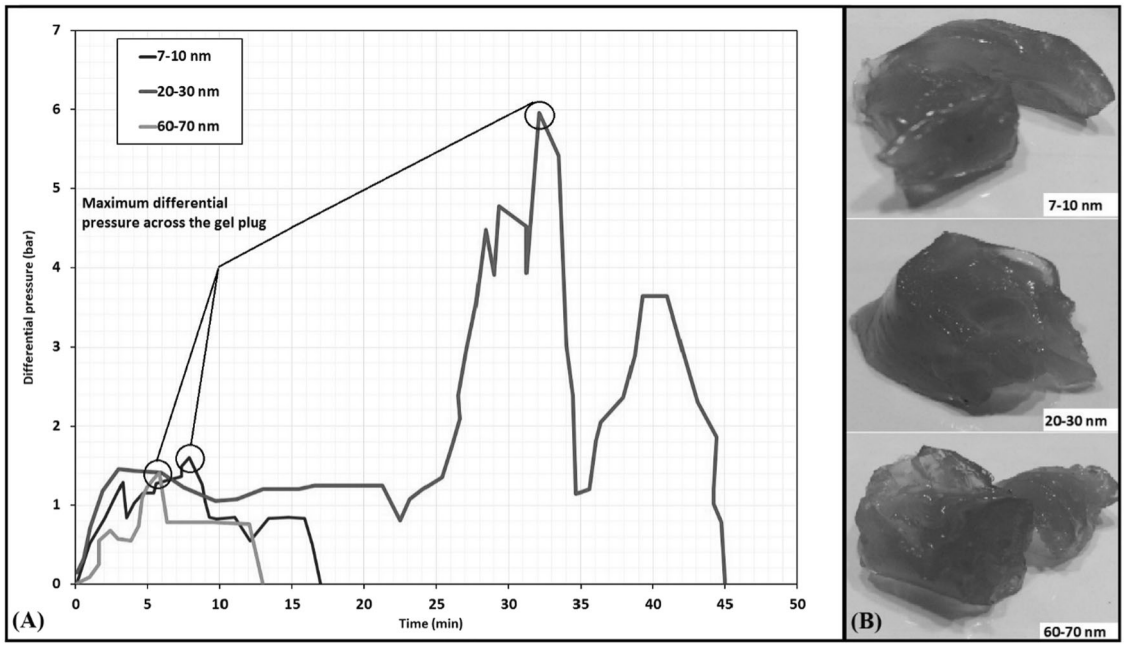


**Fig. 11** **(a)** Differential pressure across the gel vs. time for gels numbered 4, 8 and 12. In all tests, the gel column length and diameter were 200 mm and 25.4 mm, respectively. **(b)** Gels extracted from the threshold pressure setup after test finalization showing the structure of the failed gels


**Fig. 12** The difference between gel columns for gel number 4, 8 and 12 after reaching their maximum DCP. The gel column length and diameter for these cases was 200 and 25.4 mm, respectively

from the steel cylinder even after reaching its maximum DCP. Moreover, on top of having a higher DCP in comparison to the other two samples, the gel column for gel number 8 kept its original shape and was not divided into smaller pieces after reaching the maximum DCP (Fig. 12b).

## Conclusion

In this study, twelve SPAM/chromium (III) acetate nanocomposite gels were synthesized based on various concentrations and sizes of silica nanoparticles. The rheology of the gelant solution, mechanical properties of the gels, and maximum DCP at the failure point for the synthesized nanocomposites were evaluated. The most important findings of this study are summarized as follows:

1. It was observed that by reducing the nanoparticle size and increasing the nanoparticle concentration, the viscosity of the gelant solutions is increased and the precrosslinking reaction is postponed.
2. The experimental results showed that by reducing the temperature, the gelation process is slowed down.
3. By increasing the nanoparticle concentration, both viscose and elastic moduli significantly increase.
4. The viscoelastic modulus for the gels containing nanoparticles with size of 20–30 nm was much higher than that for those composites with 7–10 and 60–70 nm sized nanosilica particles.
5. The results showed that the nanocomposites containing 20–30 nm particles have a higher DCP in comparison to those having 7–10 and 60–70 nm nanoparticles.

**Acknowledgements** We thank Dr. Marjan Ashrafizadeh for her great assistance with the interpretation of our results, Dr. Maral Ghahramani for comments that improved the manuscript, and the anonymous reviewers for their helpful comments and suggestions.

## Compliance with ethical standards

**Conflict of interest** The authors declare that they have no conflict of interest.

**Publisher's note:** Springer Nature remains neutral with regard to jurisdictional claims in published maps and institutional affiliations.

## References


1. Zhao G, Dai C, Li W, Yan Z, Zhao M. Research on a temporary plugging agent based on polymer gel for reservoir acidification. J Petrol Explor Prod Technol. 2016;6:465–72. https://doi.org/10.1007/s1320
2. Gano JC. Halliburton energy services inc, temporary plug system. U S Pat. 1997;5:685. 372.
3. Kang Y, Xu C, You L, Yu H, Zhang D. Temporary sealing technology to control formation damage induced by drill-in fluid loss in fractured tight gas reservoir. J Nat Gas Sci Eng. 2014;20:67–73. https://doi.org/10.1016/j.jngse.2014.06.016
4. Du G, Peng Y, Pei Y, Zhao L, Wen Z, Hu Z. Thermo-responsive temporary plugging agent based on multiple phase transition supramolecular gel. Energ Fuel. 2017;31:9283–9. https://doi.org/10.1021/acs.energyfuels.7b01691
5. Liu D, Kang Y, Liu Q, Lei D, Zhang B. Laboratory research on fracture-supported shielding temporary plugging drill-in fluid for fractured and fracture-pore type reservoirs. J. Chem. 2017. https://doi.org/10.1155/2017/4176593
6. Fan X, Zhao P, Zhang Q, Zhang T, Zhu K, Zhou C. A polymer plugging gel for the fractured strata and its application. Materials. 2018;11:856 https://doi.org/10.3390/ma11050856
7. Nasiri A, Ghaffarkhah A, Moraveji MK, Gharbanian A, Valizadeh M. Experimental and field test analysis of different loss control materials for combating lost circulation in bentonite mud. J Nat Gas Sci Eng. 2017;44:1–8. https://doi.org/10.1016/j.jngse.2017.04.004
8. Nasiri A, Ghaffarkhah A, Dijvejin ZA, Mostofi M, Moraveji MK. Bridging performance of new eco-friendly lost circulation materials. Petrol Explor Dev. 2018;45:1–12.
9. Feng Y, Gray KE. Review of fundamental studies on lost circulation and wellbore strengthening. J Petrol Sci Eng. 2017;152:511–22. https://doi.org/10.1016/j.petrol.2017.01.052
10. Ezeakacha CP, Salehi S, Kiran R. Lost circulation and filter cake evolution: Impact of dynamic wellbore conditions and wellbore strengthening implications. J Petrol Sci Eng. 2018;171:1326–37. https://doi.org/10.1016/j.petrol.2018.08.063
11. Kaiser MJ. Rigless well abandonment remediation in the shallow water US Gulf of Mexico. J Petrol Sci Eng. 2017;151:94–115. https://doi.org/10.1016/j.petrol.2017.01.004
12. Yang J, Luo J, Ran JC, Wang ZP. Probe into temporary plugging technology used in low-pressure gas well for workover. Nat Gas Ind. 2007;27:81.
13. Hajipour A, Baghban Salehi M, Vafaie Sefti M, Heidari A. Experimental study of polyacrylamide gel in close-in well operation. Polym Adv Technol. 2018;29:1278–86. https://doi.org/10.1002/pat.4239
14. Aloise DJ, Aloise D, Rocha CT, Ribeiro CC, Ribeiro Filho JC, Moura LS. Scheduling workover rigs for onshore oil production. Discret Appl Math. 2006;154:695–702. https://doi.org/10.1016/j.dam.2004.09.021
15. Devold H. Oil and gas production handbook: an introduction to oil and gas production. Oslo: ABB AS; 2013.
16. Therond E, Bois AP, Whaley K, Murillo R. Large-scale testing and modeling for cement zonal isolation in water-injection wells. Spe Drill Complet. 2017. https://doi.org/10.2118/181428-PA
17. Okromelidze GV, Garshina OV, Nekrasova IL, Iljyasov SE. Method of well-killing operation by using viscoelastic gels with controllable destruction terms. In: Lie K-A, Alvarado V, Aguilera R, Fassihi R, editors. SPE Russian Oil and Gas Exploration & Production Technical Conference and Exhibition. Russia: Society of Petroleum Engineers; 2014.
18. KANG Yili, Chengyuan XU, TANG Long, Song LI, Daqi LI. Constructing a tough shield around the wellbore: theory and method for lost-circulation control. Petrol Explor Dev. 2014;41:520–7. https://doi.org/10.1016/S1876-3804(14)60061-6
19. Pei Y, Zhao L, Du G, Li N, Xu K, Yang H. Investigation of the degradation and stability of acrylamide-based polymers in acid solution: functional monomer modified polyacrylamide. Petroleum. 2016;2:399–407. https://doi.org/10.1016/j.petlm.2016.08.006
20. Arthur JD, Hochheiser HW. Plugging and abandonment of oil and gas wells. Working document of the NPC North American Resource Development Study. National petroleum Council; 2016. https://www.npcorg/prudent_development-topic_papers/2-25_well_plugging_and_abandonment_paper.pdf (2016)
21. Hossain ME, Wajheeuddin M. The use of grass as an environmentally friendly additive in water-based drilling fluids. Petrol Sci. 2016;13:292–303. https://doi.org/10.1007/s12182-016-0083-8
22. Majid NFF, Katende A, Ismail I, Sagala F, Sharif NM, Yunus MAC. A comprehensive investigation on the performance of durian rind as a lost circulation material in water based drilling mud. Petroleum. 2018. https://doi.org/10.1016/j.petlm.2018.10.004
23. Nasiri A, Shahrabi MA, Moraveji MK. Application of new eco-friendly LCMs for combating the lost circulation in heavy-weight and oil-based mud. Rsc Adv. 2018;8:9685–96. https://doi.org/10.1039/C7RA13668D
24. Liu G, Jiang H, Li J, Wang M, Chen F, Ding S, et al. Evaluation of the performance of polymer gels mixed with asphalt particle as a novel composite profile control system. J Ind Eng Chem. 2015;25:309–14. https://doi.org/10.1016/j.jiec.2014.11.044
25. Bozong H. Microscopic mechanisms and model design of close packing theory. Petrol. Drill Tech. 2007;35:5.
26. Cai J, Wu X, Gu S Research on environmentally safe temporarily plugging drilling fluid in water well drilling. In: Asia Pacific Health, Safety, Security and Environment Conference and Exhibition in Jakarta, Indonesia, 4–6 August 2009.
27. Uguna G, Rachid R, Milne A, Ali S. Controlling losses when recompleting low-pressure reservoirs. SPE European Formation Damage Conference and Exhibition, 3–5 June, Budapest, Hungary; 2015.
28. Wang G, Cao C, Pu X, Zhao Z. Experimental investigation on plugging behavior of granular lost circulation materials in fractured thief zone. Part Sci Technol. 2016;34:392–6. https://doi.org/10.1080/02726351.2015.1089963
29. Shaarpour M. Method and composition for preventing or treating lost circulation. US patent US7066285B2, Halliburton Energy Services Inc.; 2006.
30. Alsaba M, Al Dushaishi MF, Nygaard R, Nes OM, Saasen A. Updated criterion to select particle size distribution of lost circulation materials for an effective fracture sealing. J Petrol Sci Eng. 2017;149:641–8. https://doi.org/10.1016/j.petrol.2016.10.027.
31. Solomon O, Adewale D, Anyanwu C. Fracture width prediction and loss prevention material sizing in depleted formations using artificial intelligence. Nigeria Annual International Conference and Exhibition. Soc. Petrol. Eng. J. 2017. https://doi.org/10.2118/189068-MS
32. Razavi O, Vajargah AK, van Oort E, Aldin M, Govindarajan S. Optimum particle size distribution design for lost circulation

control and wellbore strengthening. J Nat Gas Sci Eng. 2016;35:836–50. https://doi.org/10.1016/j.jngse.2016.08.038
33. Ravi K, Bosma M, Gastebled O. Improve the economics of oil and gas wells by reducing the risk of cement failure. IADC/SPE Drilling Conference, 26–28 February, Dallas, TX; 2002.
34. Mangadlao JD, Cao P, Advincula RC. Smart cements and cement additives for oil and gas operations. J Petrol Sci Eng. 2015;129:63–76. https://doi.org/10.1016/j.petrol.2015.02.009
35. Brufatto C, Cochran J, Conn L, Power D, SZAA El-Zeghaty, Fraboulet B, et al. From mud to cement—building gas wells. Oilfield Rev. 2003;15:62–76.
36. Nelson EB. Well cementing. 2nd ed. Sugar Land, TX: Schlumberger Dowell; 2006.
37. Liu H, Bu Y, Sanjayan J, Shen Z. Effects of chitosan treatment on strength and thickening properties of oil well cement. Constr Build Mater. 2015;75:404–14. https://doi.org/10.1016/j.conbuildmat.2014.11.047
38. Smith RC. Improved method of setting successful cement plugs. J Petrol Technol. 1984;36:1–897. https://doi.org/10.2118/11415-PA
39. Santra AK, Kulakofsky D. Carbon dioxide-resistant Portland based cement composition. US patent US20130048284A1, Halliburton Energy Services Inc.; 2017.
40. Abid K, Gholami R, Choate P, Nagaratnam BH. A review on cement degradation under CO2-rich environment of sequestration projects. J Nat Gas Sci Eng. 2015;27:1149–57. https://doi.org/10.1016/j.jngse.2015.09.061
41. Crawshaw JP, Frigaard I. Cement plugs: stability and failure by buoyancy-driven mechanism. Offshore in Europe Oil and Gas Exhibition and Conference, 7–10 September, Aberdeen, UK.
42. Ukaji M, Takamura M, Shirai K, Gang W, Yamauchi T, Tsubokawa N. Curing of epoxy resin by hyperbranched poly (amidoamine)-grafted silica nanoparticles and their properties. Polym J. 2008;40:607.
43. Bai B, Zhou J, Yin M. A comprehensive review of polyacrylamide polymer gels for conformance control. Petrol Explor Dev. 2015;42:525–32. https://doi.org/10.1016/S1876-3804(15)30045-8
44. Farasat A, Sefti MV, Sadeghnejad S, Saghafi HR. Mechanical entrapment analysis of enhanced preformed particle gels (PPGs) in mature reservoirs. J Petrol Sci En. 2017;157:441–50. https://doi.org/10.1016/j.petrol.2017.07.028
45. Onorato J, Pakhnyuk V, Luscombe CK. Structure and design of polymers for durable, stretchable organic electronics. Polym J. 2017;49:41 https://doi.org/10.1038/pj.2016.76
46. Farasat A, Sefti MV, Sadeghnejad S, Saghafi HR. Effects of reservoir temperature and water salinity on the swelling ratio performance of enhanced preformed particle gels. Korean J Chem Eng. 2017;34:1509–16. https://doi.org/10.1007/s11814-017-0017-1
47. Glushkov DO, Lyrshchikov SY, Shevyrev SA, Strizhak PA. Burning properties of slurry based on coal and oil processing waste. Energ Fuel. 2016;30:3441–50. https://doi.org/10.1021/acs.energyfuels.5b02881
48. Novel WilsonA. Thermally stable fluid-loss pill performs better than guar-based gels. J Petrol Technol. 2013;65:134–6.A. https://doi.org/10.2118/1113-0134-JPT
49. Gamage P, Deville JP, Sherman J. Solids-free fluid-loss pill for high-temperature reservoirs. Spe Drill Complet. 2014;29:125–30. P. https://doi.org/10.2118/164064-PA
50. Ziad AB, Gromakovskii D, Al-Sagr A, Al-Driweesh S. First successful application of temporary gel plug replacing calcium carbonate chips to isolate depleted reservoir, case study from Saudi Arabia Gas Field. SPE International Conference and Exhibition on Formation Damage Control, 24–26 February, Lafayette, LO, USA.
51. Ashrafizadeh M, Ahmad RS, Sadeghnejad S. Improvement of polymer flooding using in-situ releasing of smart nano-scale coated polymer particles in porous media. Energy Explor Exploit. 2012;30:915–39. https://doi.org/10.1260/0144-5987.30.6.915
52. Ashrafizadeh M, SA AR, Sadeghnejad S. Enhanced polymer flooding using a novel nano-scale smart polymer: Experimental investigation. Can J Chem Eng. 2017;95:2168–75. https://doi.org/10.1002/cjce.22860
53. Jia H, Chen H. The potential of using $Cr^3$ + /salt-tolerant polymer gel for well workover in low-temperature reservoir: laboratory investigation and pilot test. SPE Prod Oper. 2018. https://doi.org/10.2118/189460-PA
54. Imran AB, Seki T, Takeoka Y. Recent advances in hydrogels in terms of fast stimuli responsiveness and superior mechanical performance. Polym J. 2010;42:839.
55. Kadam Y, Pochat-Bohatier C, Sanchez J, El Ghzaoui A. Modulating viscoelastic properties of physically crosslinked self-assembled gelatin hydrogels through optimized solvent conditions. J Dispers Sci Technol. 2015;36:1349–56. https://doi.org/10.1080/01932691.2014.984721
56. Azimi Dijvejin Z, Ghaffarkhah A, Vafaie Sefti M, Moraveji MK. Synthesis, structure and mechanical properties of nanocomposites based on exfoliated nano magnesium silicate crystal and poly (acrylamide). J Dispers Sci Technol. 2018. https://doi.org/10.1080/01932691.2018.1467777
57. Liang Z, Liu C, Li L, Xu P, Luo G, Ding M, et al. Double-network hydrogel with tunable mechanical performance and biocompatibility for the fabrication of stem cells-encapsulated fibers and 3D assemble. Sci Rep-Uk. 2016;6:33462.
58. Koyama Y. Synthesis of topologically crosslinked polymers with rotaxane-crosslinking points. Polym J. 2014;46:315.
59. Haraguchi K, Takehisa T. Nanocomposite hydrogels: a unique organic–inorganic network structure with extraordinary mechanical, optical, and swelling/de-swelling properties. Adva Mater. 2002;14:1120–4. https://doi.org/10.1002/1521-4095(20020816)14:16 < 1120::AID-ADMA1120 > 3.0.CO;2-9
60. Kargarzadeh H, Mariano M, Huang J, Lin N, Ahmad I, Dufresne A, et al. Recent developments on nanocellulose reinforced polymer nanocomposites: a review. Polymer. 2017. https://doi.org/10.1016/j.polymer.2017.09.043
61. Jain R, Mahto V, Sharma VP. Evaluation of polyacrylamide-grafted-polyethylene glycol/silica nanocomposite as potential additive in water based drilling mud for reactive shale formation. J Nat Gas Sci Eng. 2015;26:526–37. https://doi.org/10.1016/j.jngse.2015.06.051
62. D'Arienzo M, Redaelli M, Callone E, Conzatti L, Di Credico B, Dirè S, et al. Hybrid SiO 2@ POSS nanofiller: a promising reinforcing system for rubber nanocomposites. Mater Chem Front. 2017;1:1441–52.M. https://doi.org/10.1039/C7QM00045F
63. Hanifpour A, Bahri-Laleh N, Nekoomanesh-Haghighi M, Karimi M. Synthesis and characterization of poly1-hexene/silica nanocomposites. Polym Test. 2017;61:27–34. https://doi.org/10.1016/j.polymertesting.2017.05.002
64. Yu B, Kang W, Sarsenbekuly B, Yang R, Fan H, Yin X. Thickening behavior and synergistic mechanism of mixed system of two hydrophobically associating polymers. J Dispers Sci Technol. 2017;38:1196–203.
65. Gaharwar AK, Rivera C, Wu CJ, Chan BK, Schmidt G. Photocrosslinked nanocomposite hydrogels from PEG and silica nanospheres: structural, mechanical and cell adhesion characteristics. Mater Sci Eng C. 2013;33:1800–7. https://doi.org/10.1016/j.msec.2012.12.099
66. Wu L, Zeng L, Chen H, Zhang C. Effects of silica sol content on the properties of poly (acrylamide)/silica composite hydrogel. Polym Bull. 2012;68:309–16. https://doi.org/10.1007/s00289-011-0536-6
67. Zhao W, Li X, Gao S, Feng Y, Huang J. Understanding mechanical characteristics of cellulose nanocrystals reinforced PHEMA

nanocomposite hydrogel: in aqueous cyclic test. Cellulose. 2017;24:2095–110. https://doi.org/10.1007/s10570-017-1244-7
68. Koohi AD, Moghaddam AZ, Sefti MV, Moghadam AM. Swelling and gelation time behavior of sulfonated polyacrylamide/chromium triacetate hydrogels. J Macromol Sci B. 2011;50:1905–20. https://doi.org/10.1080/00222348.2010.549419
69. Zhu D, Bai B, Hou J. Polymer gel systems for water management in high-temperature petroleum reservoirs: a chemical review. Energy Fuels. 2017;31:13063–87. https://doi.org/10.1021/acs.energyfuels.7b02897
70. Aalaie J, Vasheghani-Farahani E, Rahmatpour A, Semsarzadeh MA. Effect of montmorillonite on gelation and swelling behavior of sulfonated polyacrylamide nanocomposite hydrogels in electrolyte solutions. Eur Polym J. 2008;44:2024–31. https://doi.org/10.1016/j.eurpolymj.2008.04.031
71. Zhu D, Hou J, Wei Q, Chen Y. Development of a high-temperature-resistant polymer-gel system for conformance control in Jidong oil field. SPE Reserv Eval Eng. 2018. https://doi.org/10.2118/186235-PA
72. Nowak AP, Sato J, Breedveld V, Deming TJ. Hydrogel formation in amphiphilic triblock copolypeptides. Supramol Chem. 2006;18:423–7. https://doi.org/10.1080/10615800600659105
73. Czerner M, Fellay LS, Suárez MP, Frontini PM, Fasce LA. Determination of elastic modulus of gelatin gels by indentation experiments. Proc Mat Sci 2015. https://doi.org/10.1016/j.mspro.2015.04.075
74. Haraguchi K. Synthesis and properties of soft nanocomposite materials with novel organic/inorganic network structures. Polym J. 2011;43:223.
75. Mohammadi S, Vafaie Sefti M, Baghban Salehi M, Mousavi Moghadam A, Rajaee S, Naderi H. Hydrogel swelling properties: comparison between conventional and nanocomposite hydrogels for water shutoff treatment. Asia. Pac J Chem Eng. 2015;10:743–53. https://doi.org/10.1002/apj.1912
76. Karnib M, Kabbani A, Holail H, Olama Z. Heavy metals removal using activated carbon, silica and silica activated carbon composite. Enrgy Proced. 2014;50:113–20. https://doi.org/10.1016/j.egypro.2014.06.014
77. Choi J, Shin H, Yang S, Cho M. The influence of nanoparticle size on the mechanical properties of polymer nanocomposites and the associated interphase region: a multiscale approach. Compos Struct. 2015;119:365–376. https://doi.org/10.1016/j.compstruct.2014.09.014
78. Jang JS, Bouveret B, Suhr J, Gibson RF. Combined numerical/experimental investigation of particle diameter and interphase effects on coefficient of thermal expansion and young's modulus of SiO2/epoxy nanocomposites. Polym Compos. 2012;33:1415–23. https://doi.org/10.1002/pc.22268
79. Liu H, Brinson LC. Reinforcing efficiency of nanoparticles: A simple comparison for polymer nanocomposites. Compos Sci Technol. 2008;68:1502–12.
80. Zare Y. Study of nanoparticles aggregation/agglomeration in polymer particulate nanocomposites by mechanical properties. Compos Part A-Appl S Manuf. 2016;84:158–64. https://doi.org/10.1016/j.compositesa.2016.01.020
81. Zare Y. The roles of nanoparticles accumulation and interphase properties in properties of polymer particulate nanocomposites by a multi-step methodology. Compos Part A Compos Part A-Appl S Manuf. 2016;91:127–32. https://doi.org/10.1016/j.compositesa.2016.10.003
82. Wang J, He YS, Yang J. Sulfur-based composite cathode materials for high-energy rechargeable lithium batteries. Adv Mat. 2015;27:569–75. https://doi.org/10.1002/adma.201402569
83. Wang C, Sun D, Zhuo K, Zhang H, Wang J. Simple and green synthesis of nitrogen, sulfur, and phosphorus-co-doped carbon dots with tunable luminescence properties and sensing application. RSC Adv. 2014;4:54060–5. https://doi.org/10.1039/C4RA10885J
84. Jin F, Feng M, Huang X, Long C, Jia K, Liu X. Effect of SiO2 grafted MWCNTs on the mechanical and dielectric properties of PEN composite films. Appl Surf Sci. 2015;357:704–11. https://doi.org/10.1016/j.apsusc.2015.09.086
85. Shokri B, Firouzjah MA, Hosseini SI. FTIR analysis of silicon dioxide thin film deposited by metal organic-based PECVD. Vol. 2631. In: von Keudell A and Winter J, editors. Proceedings of 19th International Symposium on Plasma Chemistry Society. Bochum, Germany: Center for Plasma Science and Technology (CPST), Ruhr-University Bochum; 2009.
86. Tian Q, Zhao X, Tang X, Zhang Y. Hydrophobicity of fluoro-containing physical crosslinkage domains in hydrophobically modified poly (acrylic acid) gels. J Polym Sci Phys. 2002;40:1236–44. https://doi.org/10.1002/polb.10182
87. Kiefer J, Wagenfeld S, Kerlé D. Chain length effects on the vibrational structure and molecular interactions in the liquid normal alkyl alcohols. Spectrochim Acta A. 2018;189:57–65. https://doi.org/10.1016/j.saa.2017.07.061
88. Crupi V, Majolino D, Migliardo P, Venuti V, Wanderlingh U. A FT-IR absorption analysis of vibrational properties of water encaged in NaA zeolites: evidence of a "structure maker" role of zeolitic surface. Eur Phys J E. 2003;12:55–58. https://doi.org/10.1140/epjed/e2003-01-014-4
89. Crupi V, Majolino D, Migliardo P, Venuti V. Diffusive relaxations and vibrational properties of water and H-bonded systems in confined state by neutrons and light scattering: state of the art. J Phys Chem A. 2000;104:11000–12. https://doi.org/10.1021/jp001736l
90. Fahmy A, Eisa WH, Yosef M, Hassan A. Ultra-thin films of poly (acrylic acid)/silver nanocomposite coatings for antimicrobial applications. J. Spectrosc. 2016. https://doi.org/10.1155/2016/7489536
91. Magalhães ASG, Almeida Neto MP, Bezerra MN, Ricardo NM, Feitosa J. Application of FTIR in the determination of acrylate content in poly (sodium acrylate-co-acrylamide) superabsorbent hydrogels. Quím Nova. 2012;35:1464–7. https://doi.org/10.1590/S0100-40422012000700030
92. Okay O, Gürün Ç. Formation and structural characteristics of porous ethylene glycol dimethacrylate networks. J Appl Polym Sci. 1992;46:421–34. https://doi.org/10.1002/app.1992.070460307
93. Hu Z, Haruna M, Gao H, Nourafkan E, Wen D. Rheological properties of partially hydrolyzed polyacrylamide seeded by nanoparticles. Ind Eng Chem Res. 2017;6:3456–63.
94. Zhao F, Yao D, Guo R, Deng L, Dong A, Zhang J. Composites of polymer hydrogels and nanoparticulate systems for biomedical and pharmaceutical applications. Nanomaterials. 2015;5:2054–130. https://doi.org/10.3390/nano5042054
95. Oun AA, Rhim JW. Carrageenan-based hydrogels and films: effect of ZnO and CuO nanoparticles on the physical, mechanical, and antimicrobial properties. Food Hydrocoll. 2017;67:45–53. https://doi.org/10.1016/j.foodhyd.2016.12.040